How to cite: *Angew. Chem. Int. Ed.* **2025**, e202503828
doi.org/10.1002/anie.202503828

Aldehyde Oxidation

High-Performance Cu_6Sn_5 Alloy Electrocatalysts for Formaldehyde Oxidative Dehydrogenation and Bipolar Hydrogen Production

Xiaoyang Fu, Dongfang Cheng, Ao Zhang, Jingxuan Zhou, Sibo Wang, Chengzhang Wan, Xun Zhao, Jun Chen, Philippe Sautet, Yu Huang,* and Xiangfeng Duan**

Abstract: Aldehyde-assisted water electrolysis offers an attractive pathway for energy-saving bipolar hydrogen production with combined faradaic efficiency (FE) of 200% while converting formaldehyde into value-added formate. Herein we report the design and synthesis of noble metal-free Cu_6Sn_5 alloy as a highly effective electrocatalyst for formaldehyde electro-oxidative dehydrogenation, demonstrating a geometric current density of 915 ± 46 mA cm^{-2} at 0.4 V versus reversible hydrogen electrode, outperforming many noble metal electrocatalysts reported previously. The formaldehyde-assisted water electrolyzer delivers 100 mA cm^{-2} at a low cell voltage of 0.124 V, and a current density of 486 ± 20 mA cm^{-2} at a cell voltage of 0.6 V without any iR compensation and exhibits nearly 200% faradaic efficiency for bipolar hydrogen production at 100 mA cm^{-2} in 88 h long-term operation. Density functional theory calculations further confirm the notably lowered barriers for dehydrogenation and Tafel steps on the Cu_6Sn_5 surface compared to Cu, underscoring its potential as a highly active catalyst.

Introduction

By replacing the anodic water oxidation reaction in conventional water electrolysis with the oxidation reactions of alternative substrates (e.g., alcohols,[1,2] hydrazine,[3] sulfide,[4] amine,[5] and urea,[6] etc.), hybrid water electrolysis substantially lowers voltage requirement and energy consumption for hydrogen production while simultaneously enabling the removal of environmental pollutants or the generation of value-added products.[7,8] Among the various substrates, aldehydes have attracted increasing interests recently for their unique electro-oxidative dehydrogenation reaction at low overpotential (Equation 1), which, when combined with the cathodic hydrogen evolution reaction (HER, Equation 2), could lead to a combined 200% faradaic efficiency (FE) for bipolar hydrogen production with 1 mole H_2 production upon 1 mole electron transfer through the external circuit (0.5 mole H_2 from cathode and anode, respectively).[9,10] Furthermore, this reaction could bring additional environmental benefits by converting formaldehyde (a common pollutant in certain industrial wastewater[11,12]) to potassium formate (a value-added commodity chemical that is ~4-fold more expensive than formaldehyde according to the export price from China to the US).[13]

$$RCHO + 2OH^- \rightarrow RCOO^- + H_2O + \frac{1}{2}H_2 + 1e^- \quad (1)$$

$$H_2O + 1e^- \rightarrow OH^- + \frac{1}{2}H_2 \quad (2)$$

With this process, the anodic electrocatalytic formaldehyde oxidative dehydrogenation (FOD) plays a vital role. Typically, Group 11 metals such as Cu, Ag, and Au[14] have been explored for the low-potential FOD reaction since their weak metal–hydrogen (M–H) binding energy is favorable for the hydrogen evolution (2H* → H_2, Tafel step) rather than the oxidation of H* that may easily take place on Pt group metals (H* + OH^- → H_2O + $1e^-$). Among the Group 11 metals, Cu is particularly attractive for its earth abundance and low cost. However, monometallic Cu electrocatalysts often exhibit limited activity and stability, leading to rapid performance decay.[10,15] Therefore, the anode electrocatalyst development remains to be a limiting challenge in this field. To this end, a number of bimetallic electrocatalysts, including CuAg,[9,16] CuAu,[17] CuPd,[17] and CuPt[17] have been explored to improve the performance and durability of Cu-based electrocatalysts. However, the introduction of these precious metals leads to substantial cost increase (over 2 order of magnitudes) compared with Cu.[18] Additionally, the hydrogen spillover and oxidation (e.g., in the case of CuPt) could also substantially lower the FE of anodic hydrogen evolution.[17]

[*] X. Fu, J. Zhou, S. Wang, C. Wan, Prof. P. Sautet, Prof. Y. Huang, Prof. X. Duan
Department of Chemistry and Biochemistry, University of California, Los Angeles, Los Angeles, CA 90095, USA
E-mail: sautet@ucla.edu
xduan@chem.ucla.edu

X. Fu, A. Zhang, C. Wan, Prof. Y. Huang
Department of Materials Science and Engineering, University of California, Los Angeles, Los Angeles, CA 90095, USA
E-mail: yhuang@seas.ucla.edu

D. Cheng, Prof. P. Sautet
Department of Chemical and Biomolecular Engineering, University of California, Los Angeles, Los Angeles, CA 90095, USA

X. Zhao, Prof. J. Chen
Department of Bioengineering, University of California, Los Angeles, Los Angeles, CA 90095, USA

Additional supporting information can be found online in the Supporting Information section

It has been suggested that the FOD typically involves the formation and adsorption of hydroxy methoxide anion ($H_2CO + OH^- \rightarrow H_2C(OH)O^-$) followed by $1e^-$ oxidation that leads to M—H bond formation and adsorbed formate.[16] Therefore, electrocatalysts that can facilitate the hydrogen production ($2H^* \rightarrow H_2$, Tafel step) and formate desorption is beneficial for the FOD reaction. Based on the volcano plot, Sn has further lowered M—H binding energy compared with Cu,[19,20] indicating it could further facilitate hydrogen desorption for anodic hydrogen production. In addition, CuSn alloy has been widely reported as CO_2 reduction reaction (CO_2RR) electrocatalysts with formate as the main product,[21–23] suggesting that the CuSn alloy could also facilitate the formate desorption upon the introduction of Sn.[16] Furthermore, the charge transfer from Sn to Cu in the CuSn alloy electrocatalysts modulates the electron density on the Cu site,[24,25] potentially benefiting catalytic reactions in general. Therefore, we designed and synthesized noble metal-free Cu_6Sn_5 alloy electrocatalysts via a facile electrodeposition method, achieving a current density of 915 ± 46 mA cm^{-2} at 0.4 V versus reversible hydrogen electrode (RHE) for FOD reaction. Furthermore, using Cu_6Sn_5 alloy as the anode electrocatalyst, the formaldehyde-assisted water electrolyzer delivers a current density of 100 mA cm^{-2} at a low voltage of 0.124 V and a current density of 486 ± 20 mA cm^{-2} at 0.6 V without any iR compensation and retains a stable nearly 200% combined FE for both anodic and cathodic hydrogen production while concurrently converting formaldehyde into value-added formate during 88 h of continued operation. Density functional theory (DFT) calculations confirm that the Cu_6Sn_5 surface can facilitate the $H_2C(OH)O^-$ adsorption, promote the dehydrogenation, *H recombination, and formate desorption, offering advantages in reaction kinetics and reduced susceptibility to site poisoning.

Results and Discussion

Synthesis and Characterization

The CuSn electrocatalysts were synthesized via a hydrogen bubble template electrodeposition method (Figure 1a) with $CuSO_4$ and $SnSO_4$ as the precursors, respectively. The as-prepared Cu_6Sn_5 electrocatalysts demonstrate branched shape morphology and Cu_6Sn_5 alloy phase (Figures S1–S3). The brached-pine shape of the Cu_6Sn_5 electrocatalysts are largely rertained after 10-h electrochemical testing, as shown in both scanning electron microscopy (SEM) and transmission electron microscopy (TEM) pictures (Figure 1b,c). The high-resolution TEM (HRTEM) shows a well-resolved lattice spacing of 0.30 nm (Figure 1d) corresponding to the (22-1) facet of the monoclinic η'-Cu_6Sn_5 alloy.[26,27] Energy dispersive X-ray spectroscopy (EDX) mapping demonstrates the uniform distribution of the Cu and Sn elements (Figure 1e–g). The X-ray diffraction (XRD) pattern confirms the η'-Cu_6Sn_5 alloy, which represents the most stable alloy phase formed between Cu and Sn under room temperature[28] and consistent with studies under similar conditions (Figure 1h).[26,27] X-ray photoelectron spectroscopy (XPS) demonstrates that Cu is mostly in Cu^0 state (Figure 1i), while surficial Sn exists mostly in the oxidized form (SnO_x) potentially attributed to air exposure (Figure 1j).[26] For comparison, the Cu electrocatalyst with a similar branched morphology was also synthesized under similar conditions with (111) facet exposed (Figure S4).[29]

Single Electrode Test

The electrochemical properties of the Cu_6Sn_5 alloy electrocatalysts were studied in a single-compartment electrochemical cell with Hg/HgO reference electrode and graphite counter electrode. We first conducted linear scan voltammetry (LSV) to evaluate the performance of the Cu_6Sn_5 alloy electrocatalysts for the FOD reaction. The LSV shows that the Cu_6Sn_5 alloy electrocatalysts demonstrate a current density of 315 ± 16 mA cm^{-2} at 0.4 V versus RHE even without iR compensation, which is considerably higher than that of Cu electrocatalysts (123 ± 6 mA cm^{-2} at 0.4 V vs. RHE) (Figure 2a). By implementing an 80% iR compensation due to the higher current density in the higher potential region (Figure S5), the Cu_6Sn_5 alloy electrocatalyst delivers a current density of 915 ± 46 mA cm^{-2} at 0.4 V versus RHE (Figure 2b), which is nearly sixfold improvement compared with Cu electrocatalysts (144 ± 8 mA cm^{-2} at 0.4 V vs. RHE). Such notable performance improvement is likely to have arisen from the synergy between Cu and Sn. In particular, the introduction of Sn could facilitate the Tafel step for H* species desorption and hydrogen evolution ($*H + *H \rightarrow H_2$) during the FOD reaction because of the weakened M—H binding energy of Sn accordingly.[19,20] Additionally, CuSn alloy electrocatalysts[21,22] and their counterpart with surficial oxides (e.g., $CuSn/SnO_x$)[23] have also been reported for CO_2RR to formate, indicating that the Sn species could be favorable for formate desorption that is also important for the FOD reaction.

We have also tested the performance of the electrodeposited Sn and found no appreciable catalytic performance for the FOD reaction (Figure S6). Furthermore, Sn showed notable self-electrooxidation, with the current rapidly decaying and Sn severely falling off from the electrode over each LSV scan (Figure S6). In contrast, the LSV curve of Cu_6Sn_5 alloy showed negligible current in the electrolyte without formaldehyde, indicating little self-electrooxidation of Sn in the Cu_6Sn_5 alloy (Figure S7). These studies have further confirmed the indispensable roles of both Cu and Sn for robust FOD reaction.

We further evaluated the electrochemical surface area (ECSA) by conducting the electric double layer capacitance measurements at different scan rates from 20 to 140 mV s^{-1} (Figures 2c and S8). The Cu_6Sn_5 alloy electrocatalysts demonstrated an ECSA of 34.9 ± 1.0 mF cm^{-2}, ~1.5 times enhancement compared with the Cu electrocatalysts (24.4 ± 1.3 mF cm^{-2}), which also generally agrees with the morphology due to the comparably fine structure. Thus, the moderate difference in ECSA (<50%) alone cannot explain the much more significant performance enhancement (~6-fold), suggesting the improvement

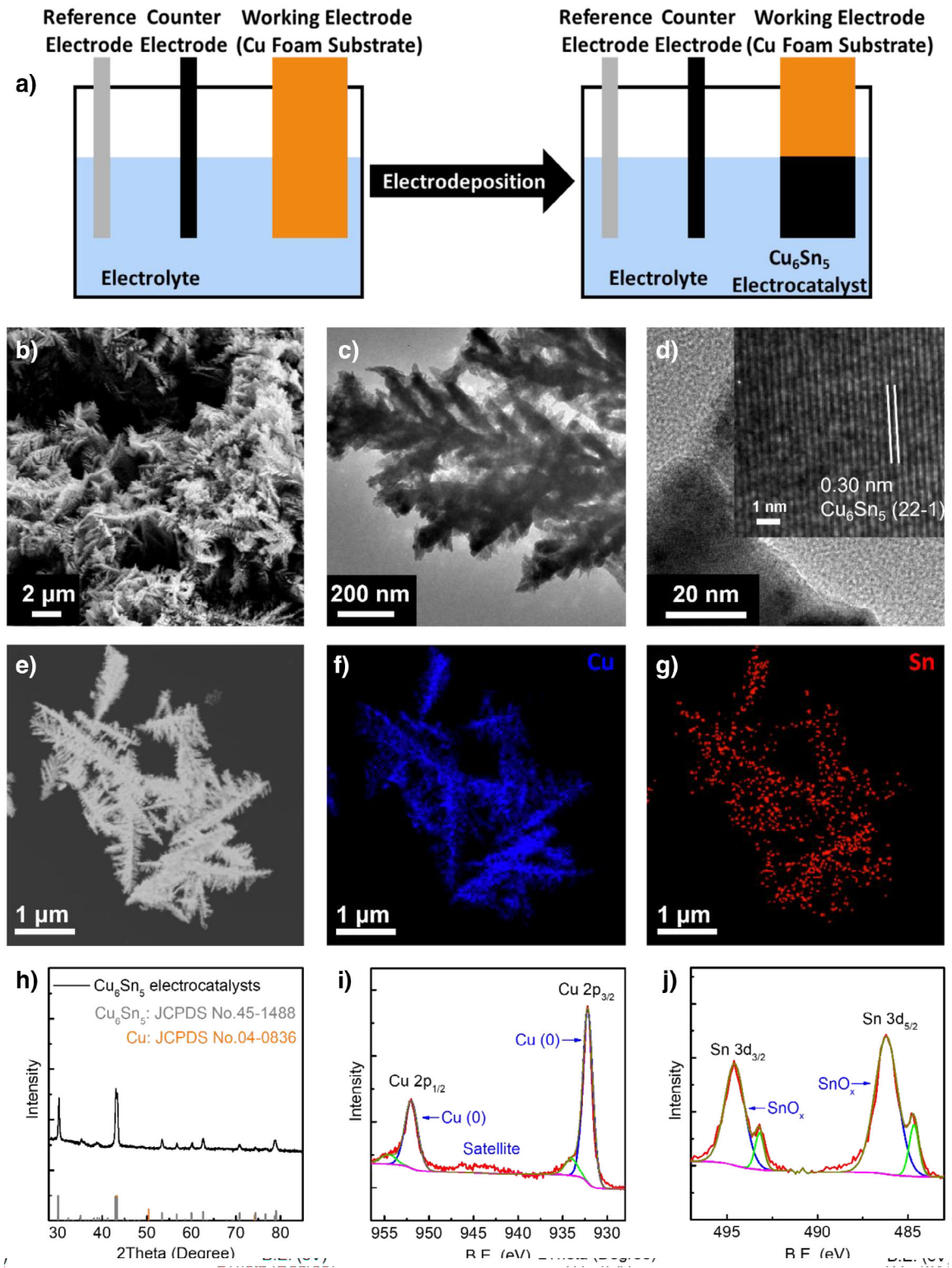

Figure 1. Synthesis and structural characterizations of the Cu_6Sn_5 electrocatalysts under working conditions. a) Schematic illustration of the Cu_6Sn_5 electrocatalyst synthesis. b) SEM image of Cu_6Sn_5 electrocatalysts. c) TEM image of Cu_6Sn_5 electrocatalysts. d) HRTEM image of Cu_6Sn_5 electrocatalysts. e) STEM image of Cu_6Sn_5 electrocatalysts. f) EDX mapping of Cu_6Sn_5 electrocatalysts (Cu element). g) EDX mapping of Cu_6Sn_5 electrocatalysts (Sn element). h) XRD pattern of Cu_6Sn_5 electrocatalysts. i) XPS study of Cu_6Sn_5 electrocatalysts (Cu 2p). j) XPS study of Cu_6Sn_5 electrocatalysts (Sn 3d).

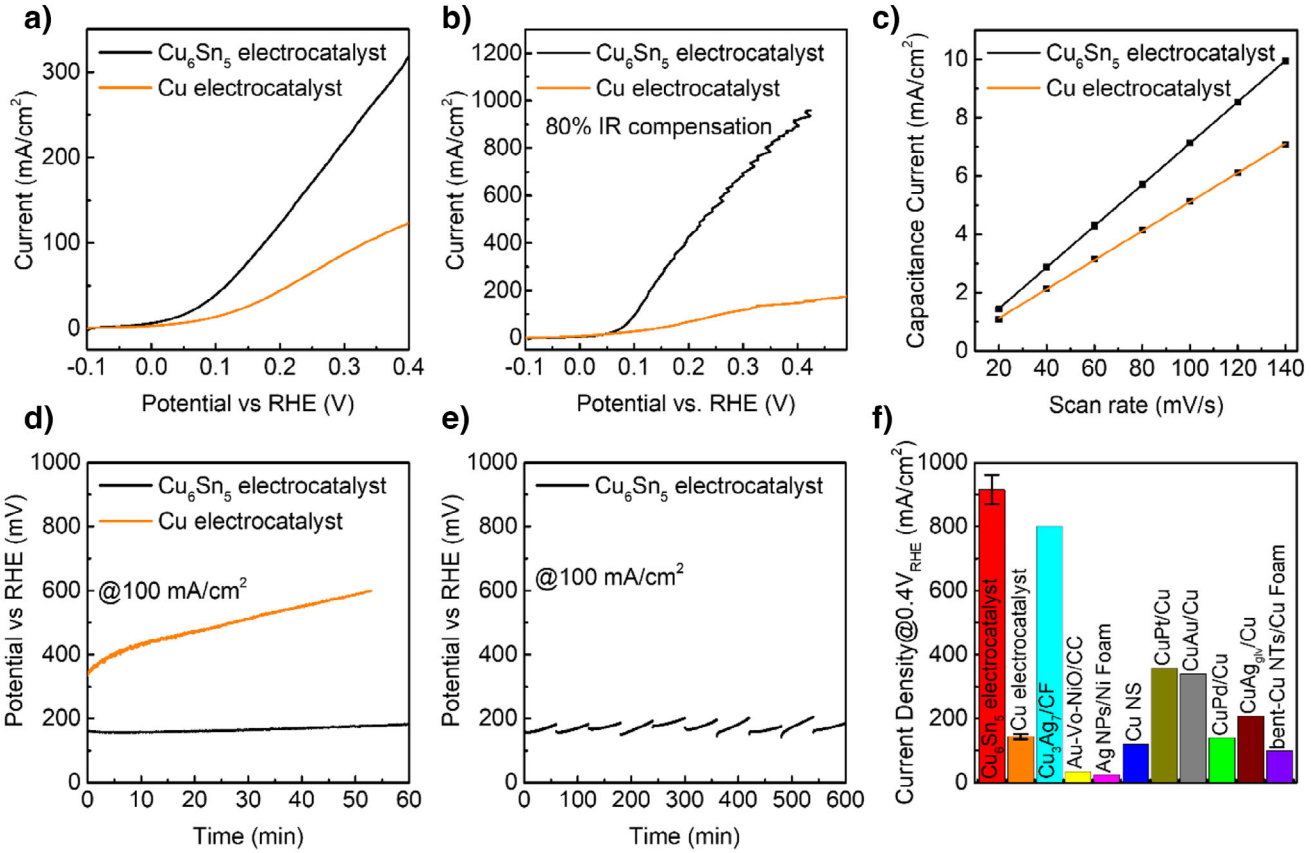

Figure 2. Single electrode test of Cu_6Sn_5 and Cu electrocatalysts. a) LSV polarization curves of Cu_6Sn_5 and Cu electrocatalysts. b) LSV polarization curves with 80% iR compensation. c) Linear fitting of the double-layer capacitance current from scan rate of 20–140 mV s^{-1}. d) CP test of Cu_6Sn_5 and Cu electrocatalysts at 100 mA cm^{-2}. e) Cumulative CP tests of Cu_6Sn_5 electrocatalysts at 100 mA cm^{-2} for 10 h. f) Summary and comparison with previously reported aldehyde electro-oxidative dehydrogenation electrocatalysts. The values and error bars are reported based on the average and standard deviation from three tests.

mostly stems from the synergy between Cu and Sn in the alloy.

We have also conducted chronopotentiometry (CP) tests to evaluate the long-term performance of the electrocatalysts. Impressively, the Cu_6Sn_5 alloy electrocatalysts demonstrate much improved long-term performance with only ~20 mV increase in required potential after 1 h CP test. In sharp contrast, Cu electrocatalysts show much more rapid performance decay with an evident ~300 mV increase within the same period (Figure 2d). In addition, the performance is also generally recoverable by refreshing the electrolyte (Figure 2e), suggesting the slightly reduced performance in CP testing may be attributed to formaldehyde consumption. Our studies further show that the formate itself will not be further oxidized by the electrocatalysts (Figure S9), which is in good agreement with previous report,[16] indicating formate was achieved selectively as a value-added product.

We further collected and measured the hydrogen gas produced from both working and counter electrodes during the CP tests via the water displacement method (e.g., 1st, 3rd, and 9th CP tests in Figure S10). Here, the FOD reaction proceeds on the working electrode with Cu_6Sn_5 electrocatalysts (Equation 1), while the HER takes place on the graphite counter electrode (Equation 2), with hydrogen being produced on both electrodes. The overall experimentally collected hydrogen gas volume agrees well with the theoretical value, indicating a combined 200% faradaic efficiency for hydrogen production. Graphite rod was specifically chosen as the counter electrode in this scenario because Pt could also catalyze the hydrogenation reaction of aldehyde,[30,31] which lowers the cathodic FE for HER. The dissolution of the electrocatalysts was also studied, for example, less than 60 μg Sn dissolution and negligible Cu dissolution (<1 μg) were found during 8th–10th CP tests, indicating limited Sn dissolution (in agreement with Figure S7), which has negligible impact on the FE measurement for hydrogen production (<0.03%).

Finally, we compared the performance of our electrocatalysts with previous reports of aldehyde electro-oxidative dehydrogenation processes (Figure 2f). Our Cu_6Sn_5 alloy electrocatalysts not only outperform Cu electrocatalysts synthesized under similar conditions with sixfold performance enhancement but also outperform the previously reported electrocatalysts, including Cu_3Ag_7 on copper foam (Cu_3Ag_7/CF),[16] Au on NiO with O vacancy/carbon cloth (Au-Vo-NiO/CC),[32] Ag nanoparticles on L-arginine etched Ni foam (Ag NPs/Ni foam),[33] Cu nanosheet arrays (Cu NS),[15] CuPt/Cu,[17] CuAu/Cu,[17] CuPd/Cu,[17] and

CuAg catalyst from the galvanic replacement on Cu foam ($CuAg_{glv}$/Cu),[9] bent Cu nanotubes grown on Cu foam (bent-Cu NTs/Cu foam)[34] in terms of the current density at 0.4 V versus RHE. This is particularly significant considering our Cu_6Sn_5 alloy electrocatalyst consists of only low-cost metals without any noble metals such as Ag, Au, Pt, Pd, etc., which is desirable for reducing the electrocatalyst costs.

Formaldehyde-Assisted Water Electrolysis for Bipolar Hydrogen Production

We have further constructed a formaldehyde-assisted water electrolyzer by combining the anodic FOD and cathodic HER together in a membrane electrode assembly (MEA) for bipolar hydrogen production, with Cu_6Sn_5 electrocatalysts and commercial PtNi/C as anode and cathode electrocatalysts, respectively.

Our MEA-type formaldehyde-assisted water electrolyzer demonstrates improved performance, achieving a current density of 100 mA cm^{-2} at a low input voltage of 0.124 V and delivering a current density of 486 ± 20 mA cm^{-2} at 0.6 V (Figure 3a), which far outperforms the counterpart with Cu anode electrocatalyst (100 mA cm^{-2} at 0.274 V and 240 ± 11 mA cm^{-2} at 0.6 V). Electrochemical impedance spectroscopy (EIS) results, fitted using the equivalent circuit (Figure 3b), show a low serial resistance of ~0.45 Ω, which is essential for high performance without iR compensation. Additionally, the electrolyzer using Cu_6Sn_5 electrocatalysts showed a considerably lower anodic charge transfer resistance (1.45 Ω) than Cu electrocatalysts (2.67 Ω), consistent with the improved performance.[35] The Cu_6Sn_5 electrocatalysts || PtNi/C electrolyzer also shows considerably more stable performance than the Cu electrocatalysts || PtNi/C electrolyzer, with more than 0.1 V lower required voltage to maintain 100 cm^{-2} current density and only around 25 mV h^{-1} performance decay (Figure 3c). Notably, the CP performance is also recoverable upon refreshing the electrolyte after each 8-h CP test, indicating the consumption of formaldehyde and hydroxide anion as the main reason for the gradual voltage increase, which also agrees with the previous literature.[16] Overall, our formaldehyde-assisted water electrolyzer could work at 100 mA cm^{-2} for 88 h and show little performance decay with only around 40 mV increase in cell voltage by comparing the 1st and 11th 8-h tests (Figure 3d).

We further analyzed the products during electrolysis. The hydrogen production from anodic and cathodic compartments was collected via water displacement method, demonstrating FE of nearly 100% anode and cathode H_2 production, respectively (Figure S12). ^{1}H NMR test reveals the formate concentration of ~0.58 M after 8 h of CP testing, indicating the conversion of formaldehyde into formate via the electro-oxidative dehydrogenation. The electrocatalysts maintained their branched morphology with the Cu_6Sn_5 phase (Figures S13 and S14), but the appearance of the Cu(200) peak at 50.4° (Figure S14) indicated Cu formation over time due to Sn dissolution in alkaline media, as also confirmed by ICP-MS analyses of the electrolyte during the 1st, 3rd, and 9th 8-h CP tests. Developing strategies to suppress Sn dissolution and improve the stability of these nonnoble metal-based electrocatalysts will be an important topic for future research.

We also compared the performance with conventional water electrolyzer (WE) with commercial IrO_x and commercial PtNi/C as the anode and cathode electrocatalysts, respectively. Our formaldehyde-assisted water electrolyzer demonstrates a decrease of 1.49 V in cell voltage requirement (Figure 3e) with a combined FE of ~200%, which can lead to substantial energy savings in hydrogen production. For example, by considering a hydrogen production rate of 3.73 mmol (h^{-1} cm^{-2}), which is equivalent to 200 mA cm^{-2} in conventional water electrolyzer or 100 mA cm^{-2} in bipolar hydrogen production, the electricity consumption for formaldehyde-assisted water electrolyzer is only 3.32 kWh kg^{-1} H_2 production, which is less than 1/10 of conventional water electrolyzer (47.9 kWh kg^{-1} H_2 production), leading to a significant saving in electricity cost of 6.78 USD kg^{-1} H_2 production (assuming the industrial electricity price of $0.152 kWh^{-1} in California) (Figure 3f) and could help achieve the DOE target of lowering the cost of hydrogen production to less than 1 USD kg^{-1} H_2 production. Furthermore, there are also additional economic benefits on the side of potassium formate production. The potassium formate has a commodity price of 850 USD ton^{-1} (Ex-Shandong), which is equivalent to 0.072 USD mol^{-1}, while the commodity price for formaldehyde is 192 USD ton^{-1} equivalent to 0.006 USD mol^{-1} (Ex-Shandong). By considering the consumption of 1 mole potassium hydroxide during the process for 1 mole of potassium formate production, and the commodity price of potassium hydroxide is 633 USD ton^{-1} (equivalent to 0.035 USD mol^{-1}), therefore, our process could still bring economic benefits for formaldehyde to potassium formate conversion. Furthermore, since the formaldehyde is present in industrial wastewater,[11] our process could also bring additional environmental benefits from the perspective of waste removal.

Finally, we also compared the required cell voltage at current density of 100 mA cm^{-2} with those of the previously reported state-of-the-art aldehyde-assisted water electrolyzer, including Cu_3Ag_7/CF,[16] Cu/Cu foam,[10] CuPt/Cu,[17] CuAu/Cu,[17] CuPd/Cu,[17] and $CuAg_{glv}$/Cu[9] (Figure 3g). Overall, our formaldehyde-assisted water electrolyzer features the lowest voltage requirement and much cheaper anode electrocatalysts since the cost of Cu and Sn is more than 2 order of magnitudes cheaper than most noble metals such as Ag, Au, Pt, Pd, etc.

DFT Calculations for Mechanistic Insights

DFT calculations were conducted to elucidate the high performance of the FOD reaction on Cu_6Sn_5. Based on the experimental observations, Cu(111) and Cu_6Sn_5(22-1) surfaces were selected as model systems (Figure 4b). Figure 4a illustrates the proposed mechanism for the FOD reaction. Initially, formaldehyde is hydrated and deprotonated in the alkaline media, yielding the $H_2C(OH)O^-$ anion. This anion is adsorbed onto the catalyst surface, where it undergoes oxidative dehydrogenation to form surface-bound *HCOOH

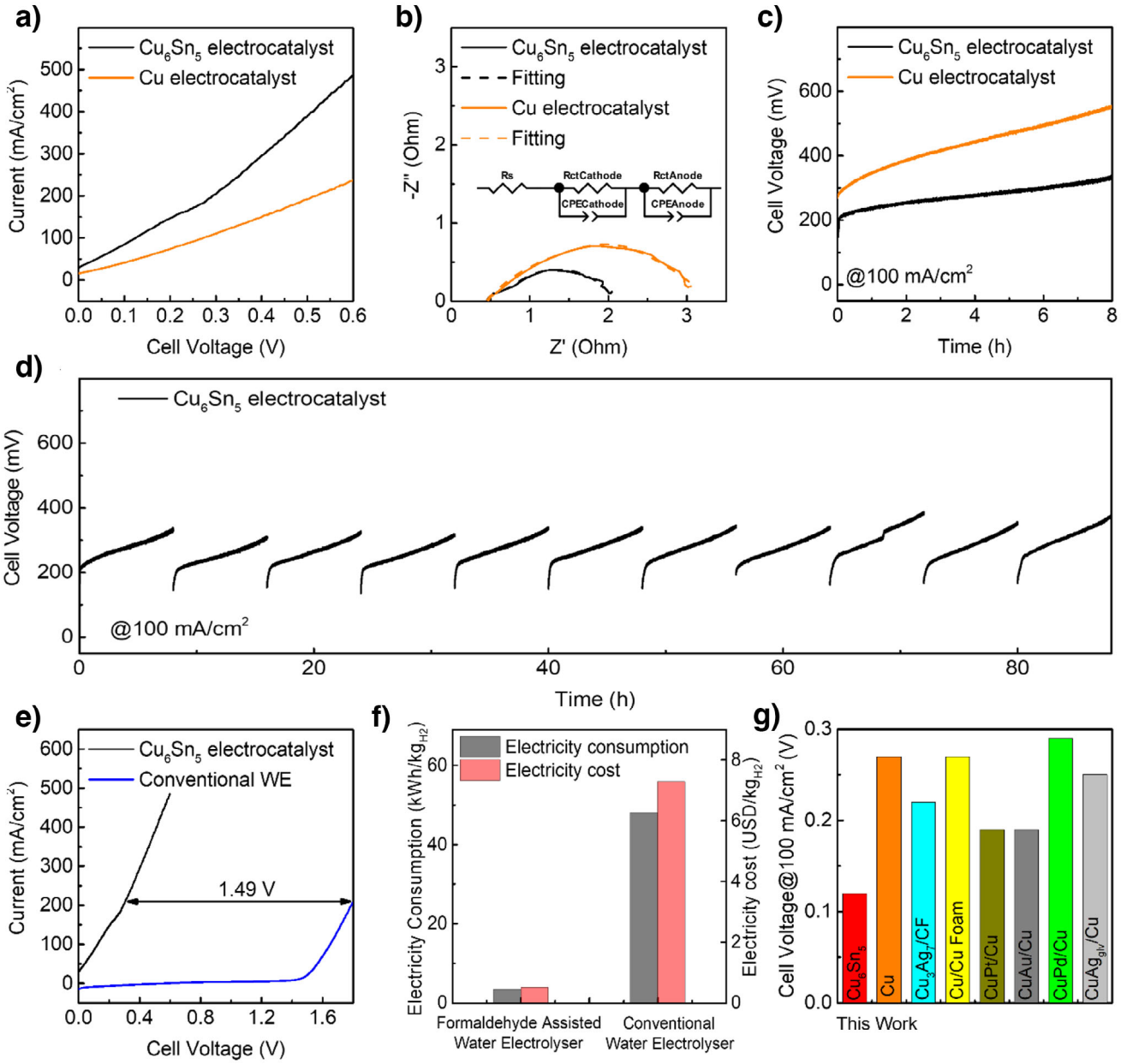

Figure 3. Formaldehyde-assisted water electrolyzer test. a) LSV polarization curves of the electrolyzer with Cu_6Sn_5 and Cu employed as anode electrocatalysts. b) EIS results of the electrolyzer s. c) CP tests of the electrolyzers at current density of 100 mA cm^{-2}. d) Cumulative CP tests of the electrolyzers with Cu_6Sn_5 as anode electrocatalysts at current density of 100 mA cm^{-2}. e) Comparisons of the polarization curves of formaldehyde-assisted water electrolyzer with conventional water electrolyzer. f) Comparison of electricity consumption and cost between formaldehyde-assisted water electrolyzer and conventional water electrolyzer at a hydrogen production rate of 3.73 mmol (h^{-1} cm^{-2}). g) Performance comparison with the previously reported state-of-the-art aldehyde-assisted water electrolyzers regarding cell voltage at 100 mA cm^{-2}. The values and error bars are reported based on the average and standard deviation from three tests.

and *H species. The *HCOOH subsequently undergoes desorption to form formate, while the *H species combine via a Tafel step to release H_2. An effective catalyst should therefore effectively adsorb $H_2C(OH)O^-$, promote its dehydrogenation, and facilitate *H recombination to minimize surface poisoning.

The adsorption of $*H_2C(OH)O$ represents a critical initial step in the dehydrogenation process, as it reflects the substrate's ability to activate and stabilize key intermediates. To this end, we examined the reaction energy for the deprotonation of H_2COHOH to $*H_2C(OH)O$ on Cu(111) and Cu_6Sn_5(22-1). As shown in Figure 4b,c, we evaluated four possible adsorption sites for $*H_2C(OH)O$ on the Cu_6Sn_5(22-1) surface. Among these, the bridge site between Cu and Sn atoms (site 4) exhibited the strongest adsorption, while adsorption on the bridge site between two Sn atoms was significantly less favorable. Furthermore, $*H_2C(OH)O$ adsorption was found to be much stronger on

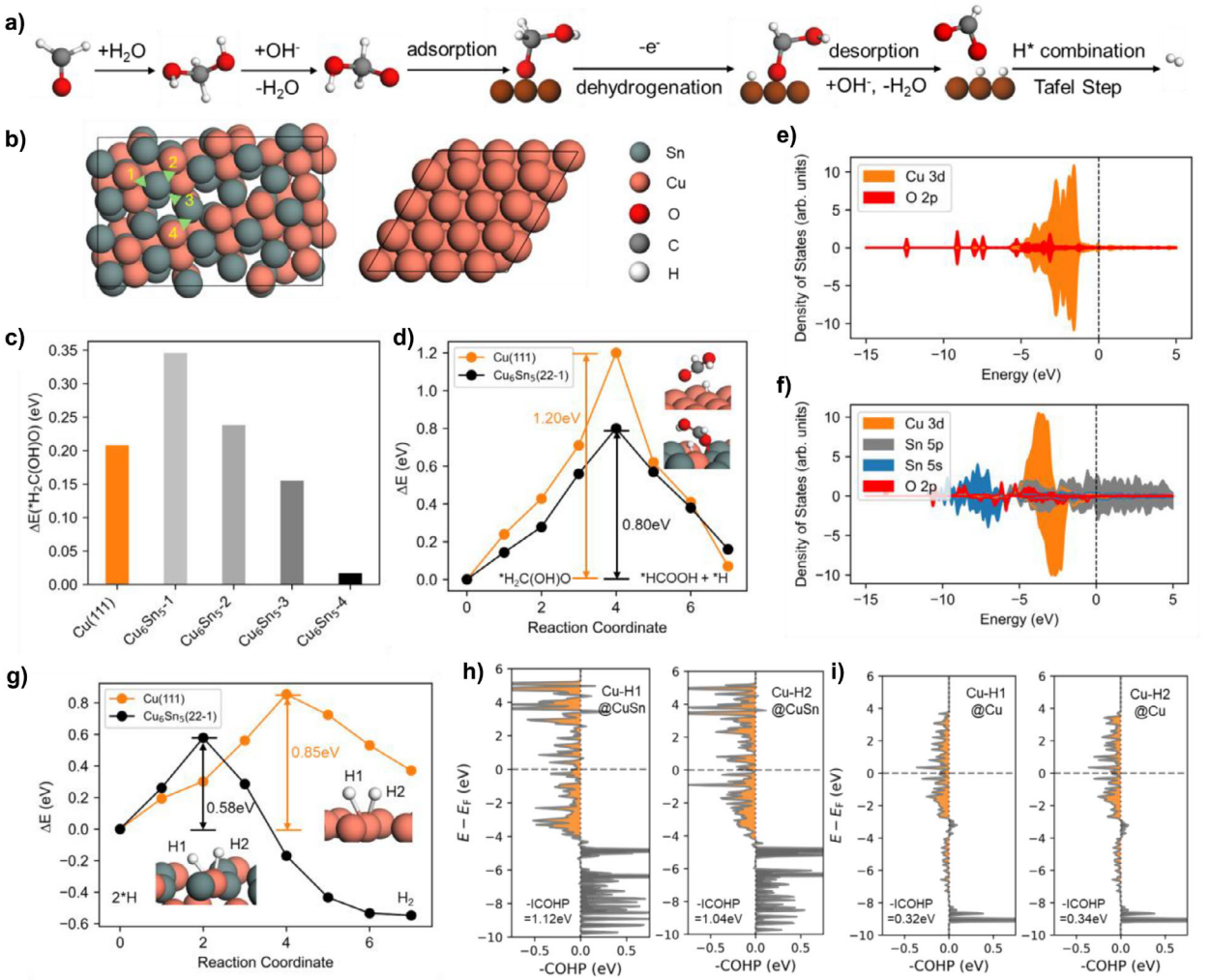

Figure 4. DFT calculations for formaldehyde oxidative dehydrogenation. a) Schematic representation of proposed reaction pathway. b) Top view of Cu_6Sn_5(22-1) and Cu(111) surface. c) Reaction energy of H_2COHOH deprotonation to $H_2C(OH)O^-$ and then adsorption. d) Reaction trajectories of $H_2C(OH)O^-$ dehydrogenation on Cu(111) and Cu_6Sn_5(22-1). e) Projected density of states of the O atom of $H_2C(OH)O$ and the Cu atom on Cu(111). f) Projected density of states of the O atom of $H_2C(OH)O$ and the Cu and Sn atoms on Cu_6Sn_5(22-1) (site 4). g) Reaction trajectories of 2*H combination to form H_2 on Cu(111) and Cu_6Sn_5(22-1) surfaces. h) Crystal orbital Hamilton population (COHP) curves for bond between Cu and H in the transition state of H combination on Cu_6Sn_5(22-1). i) Crystal orbital Hamilton population (COHP) curves for bond between Cu and H in the transition state of H combination on Cu(111).

the Cu_6Sn_5(22-1) surface compared to the hollow site on Cu(111). Analysis of the projected density of states (PDOS) for the anchored O group of $*H_2C(OH)O$ at the Cu_6Sn_5(22-1) site reveals strong orbital mixing between O 2p states and Cu 3d states from −5 to −1 eV, as well as with Sn 5p and 5s states in the ranges of −1 to 0 eV and −10 to −5 eV (Figure 4f). In contrast, on the Cu(111) surface, only Cu 3d states couple with the O 2p states (Figure 4e). The presence of additional Sn s and p states in the Cu_6Sn_5 alloy leads to enhanced orbital overlap with the O 2p states, contributing to the significantly stronger adsorption energy observed on Cu_6Sn_5(22-1).

The C─H bond cleavage, a critical step in the dehydrogenation process, is illustrated in Figure 4d. The Cu_6Sn_5(22-1) surface exhibits a substantially lower reaction barrier of 0.80 eV compared to the Cu(111) surface, where the barrier reaches 1.2 eV. This suggests that dehydrogenation is much less kinetically favorable on Cu(111). In the transition state, the O atom in *HCOOH binds with an Sn atom on the Cu_6Sn_5(22-1) surface, whereas *HCOOH remains physisorbed on the Cu(111) surface. The stronger oxophilicity and lower coordination of Sn on Cu_6Sn_5(22-1) help stabilize the transition state, thereby lowering the reaction barrier. Following the dehydrogenation step, the adsorbed *H species recombine to form H_2 gas, a process commonly known as the Tafel step. Our calculations reveal that the recombination of *H is more facile on Cu_6Sn_5(22-1), with a reaction barrier of 0.58 eV, compared to 0.85 eV on the Cu(111) surface. This indicates that H_2 formation is more kinetically sluggish on Cu(111) (Figure 4g). In this recombination step, *H─H binds to Cu sites on both Cu(111) and Cu_6Sn_5(22-1). Crystal orbital Hamilton population (COHP) analysis of the Cu─H bond reveals that Cu on the Cu_6Sn_5(22-1) surface binds *H much more strongly than Cu on the Cu(111) surface (Figure 4h,i).

Bader charge analysis reveals a partial electron transfer from Sn to Cu, resulting in a charge-rich state for Cu (0.21–0.27 e^-) (Figure S15). This analysis also generally agrees with the results from XPS (Figure S16), and the binding energy of Cu from Cu_6Sn_5 alloy electrocatalysts is lowered compared with the Cu peak from monometallic Cu, which also agrees with previous literature.[24,25] This charge accumulation on Cu helps stabilize the *H─H transition state, facilitating the hydrogen evolution step (Tafel step). This finding further supports the conclusion that the Cu_6Sn_5(22-1) surface is more active for hydrogen evolution than the pure Cu(111) surface.

Considering the potential existence of SnO_x, the catalyst model structure with surficial oxides was also constructed (Figure S17). Due to the chemical complexity of SnO_x species on the CuSn alloy surface, we simplified the model by introducing a partial oxidation state ($\frac{1}{4}$ ML oxygen relative to Sn) to explore the role of surface oxides in the catalytic reaction. The energy barriers of the hydroxy methoxide dehydrogenation step and the *H recombination step (Tafel step) on the partially oxidized Cu_6Sn_5 (22-1) surface are similar to those of Cu_6Sn_5(22-1) surface and remain lower than those on Cu(111) surface. Thus, partial oxidation of Sn appears to have minimal impact on catalytic activity. Future research focusing on in situ analysis of the surface composition of SnO_x@CuSn under realistic reaction conditions will be important for further clarifying its effect on catalytic performance.

Conclusion

In conclusion, we have designed and synthesized noble metal-free Cu_6Sn_5 alloy electrocatalyst via a facile electrodeposition method. The resulting Cu_6Sn_5 alloy exhibits excellent electrocatalytic activity for the FOD reaction, achieving a geometric current density of 915 mA cm^{-2} at 0.4 V versus RHE. Using the Cu_6Sn_5 alloy as formaldehyde dehydrogenation catalyst, we further constructed formaldehyde-assisted water electrolyzer with improved performance (486 mA cm^{-2} at 0.6 and 0.124 V at 100 mA cm^{-2} without any iR compensation) and durability, surpassing previous reports. DFT study reveals that the Cu_6Sn_5(22-1) surface exhibits superior performance across all key steps of the reaction mechanism—$H_2C(OH)O^-$ adsorption, C─H bond cleavage, and *H recombination—compared to Cu(111). This work presents an effective path for developing noble metal-free, low-cost electrocatalysts for the FOD reaction. It could enable formaldehyde-assisted water electrolysis for cost-effective bipolar hydrogen production along with effective chemical upgrading.

Acknowledgements

Y.H. acknowledges support from the National Science Foundation award 2404462. D.C. and P.S. acknowledge support from the National Science Foundation award 2103116 and Audi CO2 Cy Pres Award. D.C. used the HOFFMAN2 cluster at the UCLA Institute for Digital Research and Education (IDRE) and the Expanse cluster through the allocation CHE170060 at the San Diego Supercomputing Center through ACCESS.

Conflict of Interests

The authors declare no conflict of interest.

Data Availability Statement

The data that support the findings of this study are available from the corresponding author upon reasonable request.

Keywords: Aldehyde oxidative dehydrogenation · Cu_6Sn_5 alloy · Electrocatalysis · Electrodeposition · Hydrogen production

[1] X. Fu, C. Wan, H. Huyan, S. Wang, A. Zhang, J. Zhou, H. Zhang, X. Zhao, J. Chen, X. Pan, Y. Huang, X. Duan, *EES Catal.* **2024**, *2*, 1285–1292.
[2] Z. Li, Y. Yan, S.-M. Xu, H. Zhou, M. Xu, L. Ma, M. Shao, X. Kong, B. Wang, L. Zheng, H. Duan, *Nat. Commun.* **2022**, *13*, 147.
[3] X. Fu, D. Cheng, A. Zhang, J. Zhou, S. Wang, X. Zhao, J. Chen, P. Sautet, Y. Huang, X. Duan, *Energy Environ. Sci.* **2024**, *17*, 2279–2286.
[4] Q. Mao, X. Mu, K. Deng, H. Yu, Z. Wang, Y. Xu, X. Li, L. Wang, H. Wang, *ACS Nano* **2023**, *17*, 790–800.
[5] Y. Sun, H. Shin, F. Wang, B. Tian, C.-W. Chiang, S. Liu, X. Li, Y. Wang, L. Tang, W. A. Goddard III, M. Ding, *J. Am. Chem. Soc.* **2022**, *144*, 15185–15192.
[6] S.-K. Geng, Y. Zheng, S.-Q. Li, H. Su, X.u Zhao, J. Hu, H.-B.o Shu, M. Jaroniec, P. Chen, Q.-H. Liu, S.-Z. Qiao, *Nat. Energy* **2021**, *6*, 904–912.
[7] J.-T. Ren, L. Chen, H.-Y. Wang, W.-W. Tian, Z.-Y. Yuan, *Energy Environ. Sci.* **2024**, *17*, 49–113.
[8] H. Y. Wang, M. L. Sun, J. T. Ren, Z. Y. Yuan, *Adv. Energy Mater.* **2023**, *13*, 2203568.
[9] H. Liu, N. Agrawal, A. Ganguly, Y. Chen, J. Lee, J. Yu, W. Huang, M. Mba Wright, M. J. Janik, W. Li, *Energy Environ. Sci.* **2022**, *15*, 4175–4189.
[10] T. Wang, L. Tao, X. Zhu, C. Chen, W. Chen, S. Du, Y. Zhou, B. Zhou, D. Wang, C. Xie, P. Long, W. Li, Y. Wang, R. Chen, Y. Zou, X.-Z. Fu, Y. Li, X. Duan, S. Wang, *Nat. Catal.* **2022**, *5*, 66–73.
[11] A. Hidalgo, A. Lopategi, M. Prieto, J. Serra, M. Llama, *Appl. Microbiol. Biotechnol.* **2002**, *58*, 260–264.
[12] H. R. Lotfy, I. Rashed, *Water Res.* **2002**, *36*, 633–637.
[13] D. A. Bulushev, J. R. Ross, *ChemSusChem* **2018**, *11*, 821–836.
[14] J. Van Den Meerakker, *J. Appl. Electrochem.* **1981**, *11*, 387–393.
[15] Y. Yang, X. Wu, M. Ahmad, F. Si, S. Chen, C. Liu, Y. Zhang, L. Wang, J. Zhang, J.-L.i Luo, X.-Z. Fu, *Angew. Chem. Int. Ed.* **2023**, *62*, e202302950.
[16] G. Li, G. Han, L. Wang, X. Cui, N. K. Moehring, P. R. Kidambi, D.-e. Jiang, Y. Sun, *Nat. Commun.* **2023**, *14*, 525.
[17] H. Liu, J. Yu, Y. Chen, J. Lee, W. Huang, W. Li, *ACS Appl. Mater. Interfaces* **2023**, *15*, 37477–37485.
[18] X. Fu, C. Wan, Y. Huang, X. Duan, *Adv. Funct. Mater.* **2022**, *32*, 2106401.
[19] B. Conway, G. Jerkiewicz, *Electrochim. Acta* **2000**, *45*, 4075–4083.

[20] M. Jaksic, *J. New Mater. Electrochem. Syst.* **2000**, *3*, 153–168.
[21] B. Ning, W. Chang, M. Liu, H. Jiang, C. Li, *ChemElectroChem* **2021**, *8*, 1150–1155.
[22] J. Wang, J. Zou, X. Hu, S. Ning, X. Wang, X. Kang, S. Chen, *J. Mater. Chem. A* **2019**, *7*, 27514–27521.
[23] K. Ye, Z. Zhou, J. Shao, L. Lin, D. Gao, N. Ta, R. Si, G. Wang, X. Bao, *Angew. Chem. Int. Ed.* **2020**, *59*, 4814–4821.
[24] Y. Z. Nie, R. Nie, H. Lin, J. J. Wu, L. H. Yu, L. Liu, J. Y. Xi, *Angew. Chem. Int. Ed.* **2025**, *64*, e202420794.
[25] Y. Z. Nie, J. J. Wu, H. Chen, L. H. Yu, L. Liu, J. Y. Xi, *ACS Mater. Lett.* **2024**, *6*, 4028–4035.
[26] J. Shao, H. Jing, P. Wei, X. Fu, L. Pang, Y. Song, K.e Ye, M. Li, L. Jiang, J. Ma, R. Li, R. Si, Z. Peng, G. Wang, J. Xiao, *Nat. Energy* **2023**, *8*, 1273–1283.
[27] H. C. Shin, M. Liu, *Adv. Funct. Mater.* **2005**, *15*, 582–586.
[28] J.-H. Shim, C.-S. Oh, B.-J. Lee, D. Lee, *Inter. J. Mater. Res.* **1996**, *87*, 205–212.
[29] S. J. Kim, Y. I. Kim, B. Lamichhane, Y.-H. Kim, Y. Lee, C. R. Cho, M. Cheon, J. C. Kim, H. Y. Jeong, T. Ha, J. Kim, Y. H. Lee, S.-G. Kim, Y.-M. Kim, S.-Y. Jeong, *Nature* **2022**, *603*, 434–438.
[30] R. Hirschl, *J. Catal.* **2004**, *226*, 273–282.
[31] S. Zhao, Y. Wen, X. Peng, Y. Mi, X. Liu, Y. Liu, L. Zhuo, G. Hu, J. Luo, X. Tang, *J. Mater. Chem. A* **2020**, *8*, 8913–8919.
[32] Z. Li, Y. Zhang, Q. Yang, J. Wu, Z. Ren, F. Si, J. Zhao, J. Chen, *iScience* **2023**, *26*, 107994.
[33] Y. Zhang, J. Wu, X. Zhu, Z. Ren, J. Chen, *Appl. Catal. B* **2024**, *354*, 124093.
[34] T. Wang, Z. Huang, T. Liu, L. Tao, J. Tian, K. Gu, X. Wei, P. Zhou, L. Gan, S. Du, Y. Zou, R. Chen, Y. Li, X.-Z. Fu, S. Wang, *Angew. Chem. Int. Ed.* **2022**, *134*, e202115636.
[35] X. Fu, D. Cheng, C. Wan, S. Kumari, H. Zhang, A. Zhang, H. Huyan, J. Zhou, H. Ren, S. Wang, Z. Zhao, X. Zhao, J. Chen, X. Pan, P. Sautet, Y. Huang, X. Duan, *Adv. Mater.* **2023**, *35*, 2301533.

Manuscript received: February 15, 2025
Revised manuscript received: March 30, 2025
Accepted manuscript online: May 06, 2025
Version of record online: ■■, ■■

Research Article

Aldehyde Oxidation

X. Fu, D. Cheng, A. Zhang, J. Zhou, S. Wang, C. Wan, X. Zhao, J. Chen, P. Sautet*, Y. Huang*, X. Duan* — **e202503828**

High-Performance Cu_6Sn_5 Alloy Electrocatalysts for Formaldehyde Oxidative Dehydrogenation and Bipolar Hydrogen Production

The Cu_6Sn_5 alloy was developed as a high-performance, noble-metal-free electrocatalyst for the anodic formaldehyde oxidative dehydrogenation (FOD) reaction. When paired with the cathodic hydrogen evolution reaction (HER), it enables a formaldehyde-assisted water electrolyzer, facilitating energy-efficient bipolar hydrogen production and the generation of value-added formate.